ELSEVIER

Biophysical Chemistry 83 (1999) 197–209

Biophysical Chemistry

www.elsevier.nl/locate/bpc

Small angle X-ray scattering studies on local structure of tobacco mosaic virus RNA in solution

Yoshio Muroga[a], Yoh Sano[b,*], Hideo Inoue[b], Kayoko Suzuki[b], Tina Miyata[b], Takahiko Hiyoshi[b], Koichi Yokota[b], Yasushi Watanabe[b], Xinqi Liu[b], Sosaku Ichikawa[b], Hiroyuki Tagawa[c], Yuzuru Hiragi[d]

[a] *Department of Applied Chemistry, School of Engineering, Nagoya University, Furo-cho, Chikusa-ku Nagoya, Aichi 464-8603, Japan*
[b] *National Food Research Institute, Tsukuba City, Ibaraki 305-8642, Japan*
[c] *Department of Applied Chemistry, Nihon University, Tokyo 101-0062, Japan*
[d] *Institute for Chemical Research, Kyoto University, Uji, Kyoto 611-0011, Japan*

Received 23 August 1999; received in revised form 8 November 1999; accepted 10 November 1999

Abstract

Effects of temperature and ionic strength (S) on the local structure of tobacco mosaic virus RNA in phosphate buffer solution are studied by analyzing the small-angle X-ray scattering (SAXS) curves. The root-mean-square radius of a cross-section of RNA chain was kept at 0.845 ± 0.005 nm over a wide range of S from 0.2 to 0.003 at 20°C, whereas it gradually diminished from 0.85 to 0.61 nm when the temperature is raised from 20 to 50°C at $S = 0.2$. Nevertheless, all of SAXS curves reflecting the backbone structures were equally mimicked by theoretical ones of freely hinged rod (FHR) models, i.e. several straight rods joined with freely hinged joints in the form of a combination of the letter Y, if the constituent rod lengths in the models are adjusted. From these facts, it is suggested that the local structure of the RNA chain in aqueous solution is characterized by an essential feature that unpaired bases in the partially double-stranded helix are constantly far isolated from each other along the helix and the rod-like structure of the helix is preserved over a range of helical contents. Such a characteristic local structure of the chain is entirely collapsed in the formamide solution at 50°C.

Keywords: Tobacco mosaic virus RNA; Small angle X-ray scattering; Mean-squared radius of gyration; Kratky plot; Double-stranded helix

* Corresponding author. Tel./fax.: +81-298-38-8082.
E-mail address: yohsano@nfri.affrc.go.jp (Y. Sano)

0301-4622/99/$ - see front matter
PII: S0301-4622(99)00141-6

1. Introduction

As was recently reviewed by Butler [1], details of the structure of the tobacco mosaic virus (TMV) and the mechanism of its construction from the constituents are well established: The structure consists of a single-stranded RNA of approximately 6400 nucleotides surrounded by approximately 2100 subunits of a single type of coat protein, and the construction of TMV is performed in vitro under physiological conditions in two steps of nucleation and elongation. The nucleation is preceded by the insertion of a hairpin loop existing in the original structure of the RNA chain into the central hole of the nucleating disk and the nucleus thus produced triggers the reconstruction of the original structure of the RNA chain into the single-stranded chain. However, the reason why the reconstruction and the elongation could be smoothly propagated has not been fully understood. The RNA chain may have an original local structure which could be easily modified in response to any changes in circumstances. The first purpose of the present work was to examine the effects of temperature and ionic strength S on the mean-square radius of cross-section of a polymer chain $\langle R_{cs}^2 \rangle$ with the small-angle X-ray scattering (SAXS). $\langle R_{cs}^2 \rangle$ for the RNA chain in formamide at 50°C is also studied as a reference data.

The RNA chain in aqueous solution forms a partially double-stranded helical structure by folding one part of the chain onto the other part in its own chain [1]. In this occasion, it is conceived from the nucleotide sequence in the RNA chain [2–7] that either paired bases or unpaired bases would not be arranged in a long sequence, but be isolated from each other along the helical structure. As a result, isolated unpaired bases may be accommodated into a partially double-stranded helical region (*Region*-A), whereas few consecutive unpaired bases may form a flexible region (*Region*-B). In fact, Österberg et al. [8] have found that SAXS data of *E. Coli* 5S-RNA is consistently elucidated if the RNA chain takes the structure consisting of one large and two small double-stranded helices arranged in the form of the letter Y and joined with one flexible region. Min et al. [9] proposed a 'flower-like model' for the structure of MS2-RNA from the characterization of the fragment. Similar structures have also been proposed by Wilson et al. [7], Noller et al. [10], Holly et al. [11] and Doty et al. [12] for a part of the structure of the RNA chain.

Since the mobility of the isolated unpaired-bases in *Region*-A would be so restricted due to the adjacent paired bases, the structure of *Re-*

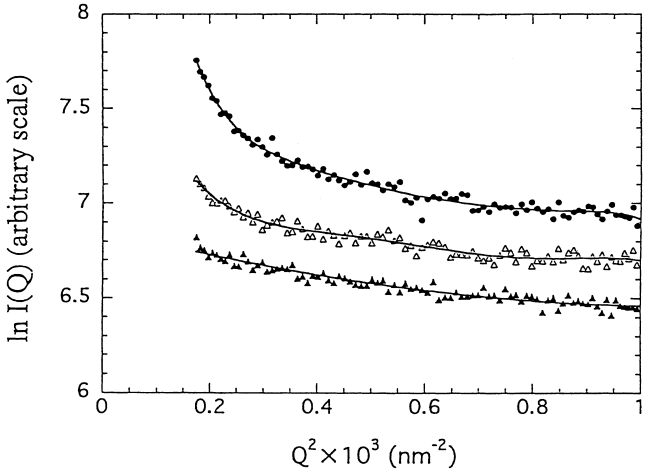

Fig. 1. Effect of pore size of filter on Guinier plot of RNA in 0.1 mol l^{-1} phosphate buffer solution ($S = 0.2$) with $C_p = 1$ mg ml^{-1}. Sample solutions were prepared with no filter (●), 1.2-μm pore sized filter (△) and 0.45-μm pore sized filter (▲).

gion-A might be approximated by a rigid rod. Therefore, it is reasonably assumed here that the backbone structure of the RNA chain could be represented by several straight rods joined with freely hinged joints in the form of a combination of the letter Y, called the freely hinged rod (FHR) model, where straight rods represent *Region*-A and freely hinged joints represent *Region*-B. The second purpose of the present work was to examine the effects of temperature and ionic strength S on the backbone structure of the RNA chain by comparing the SAXS curves, registered in a scattering vector Q ranging from 0.13 to 3.35 nm^{-1}, with theoretical scattering curves for several FHR models, where Q is defined by $Q = (4\pi/\lambda) \sin(\theta/2)$ and λ is a wavelength of X-ray and θ is a scattering angle. The scattering functions for these FHR models are computed by extending Muroga's method [13–15].

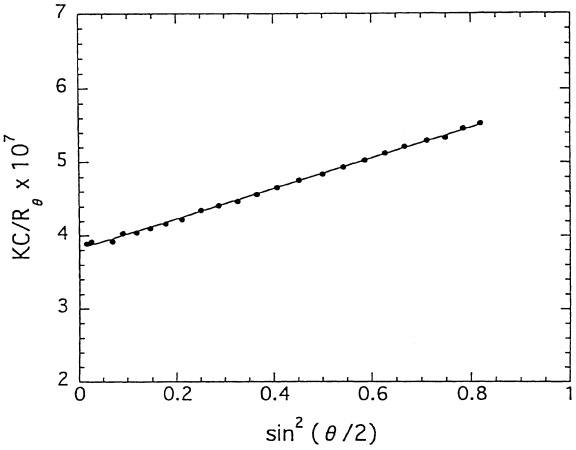

Fig. 2. Zimm plot at the dilute limit for RNA in 0.1 mol l^{-1} phosphate buffer solution ($S = 0.2$) with $C_p = 1$ mg ml^{-1}, which was prepared with 0.45-μm pore sized filter.

2. Materials and methods

2.1. Materials

Tobacco mosaic virus, Japanese common strain OM was propagated in inoculated leaves of *Nicotiana tabacum* L. ev. Xanthi and was extracted with 100 mM phosphate buffer (pH 7.0) containing 0.1% (v/v) thioglycolic acid. The virus was collected from the solution with polyethyleneglycol [16,17] and purified by two cycles of differential centrifugation. The RNA was obtained by extracting from the virus with aqueous phenol solution and bentonite, and precipitating by adding two volumes of cold ethanol to the extracted solution, followed by washing the precipitated RNA with ethanol three times. Special attention was paid to the careful sterilization of all solute and solvents in order to avoid degradation of RNA by RNAse.

In general, the RNA in aqueous solution tends to aggregate due to its high molecular weight and thus filtration is necessary to remove aggregates in the solution and prepare a sample solution dissolving monomeric RNA only. A filter (Milli-

Table 1
Root mean-square radius of cross-section for RNA chain, $\langle Rc_s^2 \rangle^{1/2}$

C_p (mg ml^{-1})	S	Temp (°C)	$\langle Rc_s^2 \rangle^{1/2}$ (nm)
4.5	0.2	20	0.85
4.5	0.2	30	0.81
4.5	0.2	40	0.76
4.5	0.2	50	0.61
4.5	0.2	20	0.85
3.32	0.05	20	0.84
3.12	0.025	20	0.84
2.95	0.003	20	0.84
5.764	Formamide	50	0.68

pore filter) having such a capacity was selected by examining both Q dependence of scattering intensity $I(Q)$ and the molecular weight of a particle dissolved in the filtrate solution with laser light scattering (LS). The details in the measurements of LS and refractive index increment are given elsewhere [18,19]. All sample solutions were dialyzed against phosphate buffer solution at 4°C right before the measurement and used immediately. The concentration of solute was determined spectrophotometrically by using an absorptivity value of 20.0 ml cm^{-1} mg^{-1} at 258 nm [20].

Fig. 1 shows the effect of pore size of filter on the Guinier plot, ln $I(Q)$ vs. Q^2 for the RNA dissolved in 0.1 mol l^{-1} phosphate buffer solution ($S = 0.2$) with the concentration $C_p = 1$ mg ml^{-1}. In the case of no filter (●) and a filter of pore-size 1.2 μm (△), their plots are not linear over an entire Q range but curve upwards at lower angles, indicating the presence of the aggregates of RNA and/or dust. In the case of a filter of pore size 0.45 μm, on the other hand, both Guinier plot (▲) in Fig. 1 and Zimm plot at the dilute limit in Fig. 2 are almost linear. Moreover, the molecular weight of a particle dissolved in the filtrated solution, which is obtained from the intercept of the Zimm plot in Fig. 2, is evaluated to be 2.6×10^6, in agreement with that of monomeric RNA [21]. Thus, filtration with a filter of pore size 0.45 μm was carried out for preparing a sample solution.

2.2. Small-angle X-ray scattering measurements and sample preparations

SAXS experiments were carried out with the optics and detector system of SAXES (small angle X-ray scattering equipment for solution samples) in the Photon Factory, KEK, Tsukuba, Japan. Scattered intensities were registered at 512 different angles in the range 0.05 $nm^{-1} < Q < 3.35$ nm^{-1} with λ of 0.1488 nm. Details in the experimental procedure are given in our previous papers [22–25]. The net scattered intensity from solute particles was obtained by subtracting the scattered intensity of blank buffer solution from that of the assembly solution.

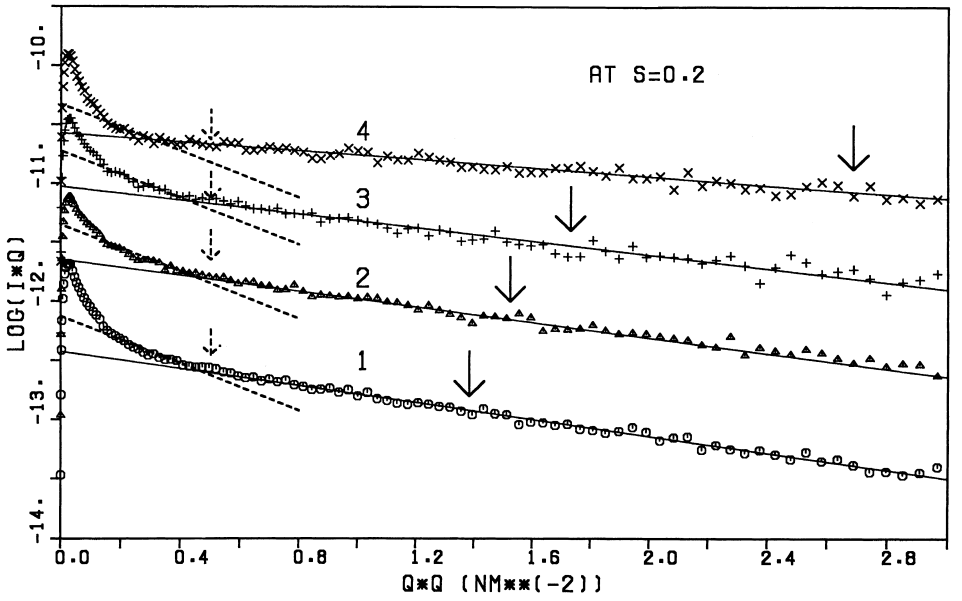

Fig. 3. Plot of $\ln(I(Q)\cdot Q)$ vs. Q^2 to evaluate mean-square radius of a cross-section of the RNA chain, $\langle R_{cs}^2 \rangle$ at 20°C (○), 30°C (△), 40°C (+) and 50°C (×) and at fixed $S = 0.2$ and $C_p = 4.5$ mg ml^{-1}. A solid arrow on each curve designates the value of Q^{*2} giving $Q^{*2}\langle R_{cs}^2 \rangle = 1$. Dotted straight lines are predicted ones giving $\langle R_{cs}^2 \rangle^{1/2}$ corresponding to the radius of a cylindrical rod, $r = 2.0$ nm and dotted arrows have the same meaning as solid arrows.

The scattered intensities from a dilute solution having $C_p = 1$ mg ml^{-1} registered with the SAXES system did not show a good enough signal-to-noise (S/N) ratio for the scattering curve to be precisely analyzed, although good S/N ratio was obtained with LS measurements. Therefore, higher C_p were employed in the SAXS measurements, as far as they are lower than the corresponding overlapping concentration C_p^* above which the solute molecules begin to overlap, since the properties of the isolated molecule are sought here.

From the slope of the Zimm plot in Fig. 2, root-mean-square radius of gyration, $\langle R_g^2 \rangle^{1/2}$ is evaluated to be 37.3 nm for the solution with $S = 0.2$. Employing the value of $\langle R_g^2 \rangle^{1/2}$ thus obtained, the corresponding C_p^* is estimated to be approximately 20 mg ml^{-1} at $S = 0.2$ by using Eq. (1):

$$C_p^* = M / \left\{ (4/3)\pi \langle R_g^2 \rangle^{3/2} A_v \right\} \quad (1)$$

where M and A_v are the molecular weight of the RNA ($= 2.6 \times 10^6$) and Avogadro's number, respectively. Since C_p^* is proportional to the inverse of intrinsic viscosity $[\eta]$ and $[\eta]$ of flexible polyelectrolyte in the presence of added salt is proportional to the inverse of $S^{1/2}$ [26], C_p^* of flexible

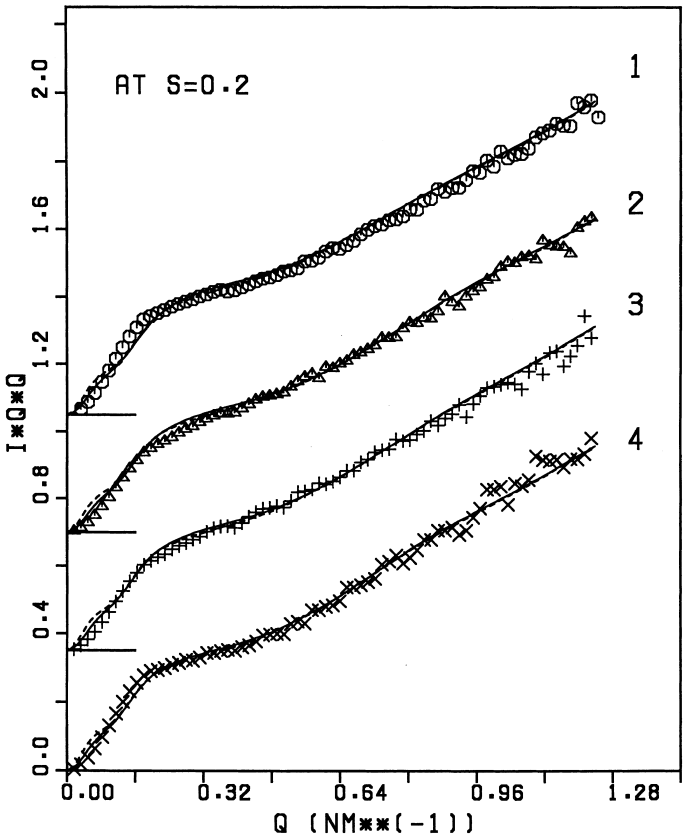

Fig. 4. (1) Comparison between observed scattering curve of RNA in aqueous solution at 20°C (○), 30°C (△), 40°C (+) and 50°C (×) and at fixed $S = 0.2$ and theoretical scattering curves for MODEL 2-1 (or 2-2) (solid curve) and MODEL 2-3 (or 2-4) (dotted curve). Rod lengths for the models are listed in Table 2. (2) Comparison between observed scattering curve of RNA in phosphate buffer solution at $S = 0.2$ (○), 0.05 (△), 0.025 (+) and 0.003 (×) and at fixed temperature of 20°C and theoretical scattering curves for MODEL 2-1 (or 2-2) (solid curve) and MODEL 2-3 (or 2-4) (dotted curve). Rod lengths for the models are listed in Table 2. (3) Comparison between the observed scattering curve of RNA in formamide solution at 50°C and the theoretical scattering curves for MODEL 2-1 (solid curve) and MODEL 2-3 (dotted curve). Rod lengths for the models are listed in Table 2.

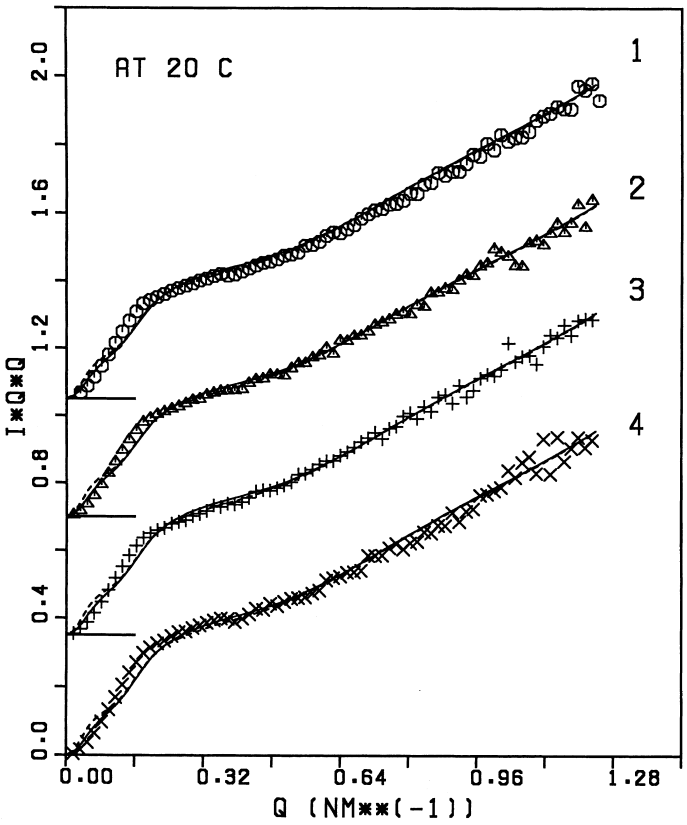

Fig. 4. (*Continued*).

polyelectrolyte would be proportional to $S^{1/2}$. Taking into account these facts, C_p^* of RNA at $S = 0.05$, 0.025 and 0.003 would be equal to or larger than approximately 10, 7.1 and 2.4 mg ml^{-1}, respectively. C_p for an each sample solution was adjusted so as to be lower than the corresponding C_p^* thus evaluated, as shown in Table 1, except for the sample with $S = 0.003$, whose C_p, 2.95 mg ml^{-1}, was slightly higher than the C_p^*, 2.4 mg ml^{-1}. C_p of RNA in the formamide solution was adjusted to 5.76 mg ml^{-1}, reasonably assuming its corresponding C_p^* would be comparable with that for the aqueous solution with $S = 0.2$, approximately 20 mg ml^{-1}.

In general, the observed scattering intensity $I(Q)$ for an isolated molecule is related to the scattering function for the molecule, $P(Q)$, through the relation $I(Q) = KMC_pP(Q)$, where K is a proportional constant. In principle therefore, observed scattering curve to be compared with theoretical scattering function could be derived by dividing $I(Q)$ with $I(0)$, where $I(0)$ is $I(Q)$ at $Q = 0$. In practice, however, extrapolation of $I(Q)$ to $Q = 0$ for the present SAXS data could not be precisely performed, because the scattering curve in a lower scattering-angle region was contaminated by the direct beam and also by intermolecular interferences especially at low S. Taking into account such effects, $I(Q)$ was not divided by $I(0)$, but multiplied by a constant factor for comparisons with the theoretical scattering function.

3. Results and discussion

In general [27], $\langle R_{cs}^2 \rangle$ is evaluated from the slope of a straight line drawn in a range of

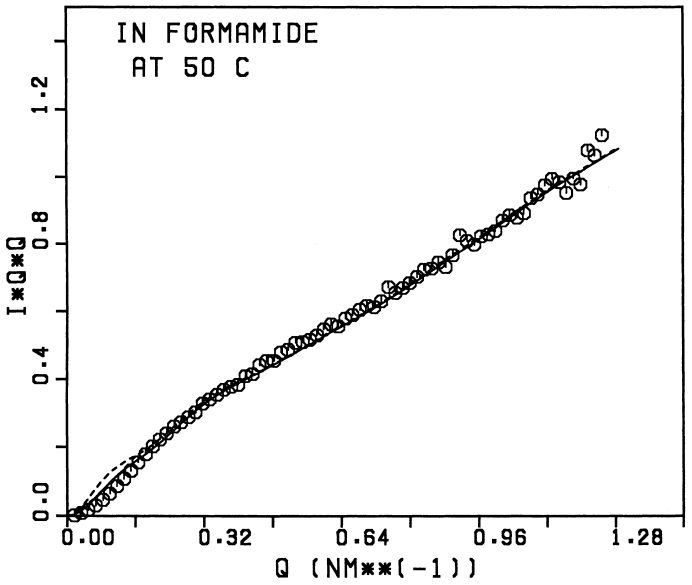

Fig. 4. (*Continued*).

$Q^2 \times \langle R_{cs}^2 \rangle < 1$ in the plot of $\ln(I(Q) \times Q)$ vs. Q^2:

$$\langle R_{cs}^2 \rangle = -2 \times (\text{slope}) \quad (2)$$

Fig. 3 shows the plot of $\ln(I(Q) \times Q)$ vs. Q^2 for RNA in 0.1 mol l^{-1} phosphate buffer solution ($S = 0.2$) at 20°C (○), 30°C (△), 40°C (+) and 50°C (×), where the data set is referred to as DS-A. Such plots for RNA in aqueous solution with various S at 20°C (DS-B) and for RNA in formamide solution at 50°C (DS-C) are similar to those of DS-A and not shown here. When $\langle R_{cs}^2 \rangle^{1/2}$ is assigned as given in Table 1, a linear relationship between $\ln(I(Q) \times Q)$ and Q^2, shown by a solid straight line in the figure, holds well far down from Q^{*2} giving $Q^{*2} \times \langle R_{cs}^2 \rangle = 1$, where a solid arrow on each curve designates the value of Q^{*2}. Upward deviation of data points in a lower Q range from the solid line can be consistently elucidated by the scattering function for a model representing the local structure of RNA chain, as is shown later.

As shown in Table 1, $\langle R_{cs}^2 \rangle^{1/2}$ of RNA chain in aqueous solution at 20°C is kept at 0.845 ± 0.005 nm over a wide range of S from 0.2 to 0.003, whereas it gradually diminished from 0.85 to 0.61 nm when the temperature was raised from 20 to 50°C at $S = 0.2$. Taking into consideration that the helical content of the RNA chain would decrease as the temperature is raised from 30 up to 80°C [28] and that increased unpaired bases would contribute to decrease $\langle R_{cs}^2 \rangle^{1/2}$, it is clear that the double-stranded helical structure tends to fray further in the latter process rather than in the former process. It should be noted here, $\langle R_{cs}^2 \rangle^{1/2}$ for RNA in formamide solution at 50°C, 6.8 nm, is comparable to that in aqueous solution at 50°C and $S = 0.2$, 6.1 nm.

It is well known [1] that the RNA chain embedded in TMV particle takes the structure of a single-stranded helix with radius $r =$ approximately 2.0 nm. The dotted straight lines in Fig. 3 are predicted if the RNA chain would take such a single-stranded helix. On this occasion, however, either upward deviation of data points in a lower Q range from the dotted straight line or another linear relationship (solid line) in a higher Q range could not be reasonably elucidated. Thus, it is evident that the RNA chain does not take such a single-stranded helix in the absence of the coat proteins.

With $\langle R_{cs}^2 \rangle^{1/2}$ listed in Table 1, $I(Q)$ is reduced to the one obtained if the RNA chain had a null cross-section, $I_{thin}(Q)$ by the relation

$I_{thin}(Q) = I(Q) \times \exp\{+1/2\langle R_{cs}^2\rangle Q^2\}$. Fig. 4-1–4-3 show the reduced Kratky plots, $I_{thin}(Q) \times Q^2$ vs. Q for the data DS-A–DS-C, respectively. In order to study the backbone structure of the RNA chain in detail, the Kratky plots thus reduced were analyzed over a Q range of 0.05–1.2 nm^{-1} by comparing them with theoretical curves obtained with scattering functions $P(Q)$ for possible FHR models, which are shown in Fig. 5. In the models, a straight rod represents a partially double-stranded helical region (*Region*-A) and a circle a small flexible region (*Region*-B), which is assumed to play the role of a freely hinged joint joining adjacent rods. Symbols A–D indicate lengths of the rods. Scattering functions $P(Q)$ for the models are computed by extending Muroga's method [13–15]. $P(Q)$ for Model 1, as an example, is given as follows:

$$
\begin{aligned}
&P(Q) \times (2A + 2B + C)^2 \\
&\quad = 2A^2 \times \left\{2\Lambda(\beta_A) - (2/\beta_A)^2 \sin^2(\beta_A/2)\right\} \\
&\qquad + 2B^2 \times \left\{2\Lambda(\beta_B) - (2/\beta_B)^2 \sin^2(\beta_B/2)\right\} \\
&\qquad + C^2 \times \left\{2\Lambda(\beta_C) - (2/\beta_C)^2 \sin^2(\beta_C/2)\right\} \\
&\qquad + 2 \times \{AB\Lambda(\beta_A)\Lambda(\beta_B) + AC\Lambda(\beta_A)\Lambda(\beta_C)\} \\
&\qquad + 2 \times \{BA\Lambda(\beta_B)\Lambda(\beta_A) + BC\Lambda(\beta_B)\Lambda(\beta_C)\} \\
&\qquad + 2 \times \{CA\Lambda(\beta_C)\Lambda(\beta_A) + CB\Lambda(\beta_C)\Lambda(\beta_B)\} \\
&\qquad + 2 \times \{A^2\Lambda^2(\beta_A)\nu_C + AB\Lambda(\beta_A)\Lambda(\beta_B)\nu_C\} \\
&\qquad + 2 \times \{B^2\Lambda^2(\beta_B)\nu_C + BA\Lambda(\beta_B)\Lambda(\beta_A)\nu_C\}
\end{aligned}
\tag{3}
$$

$$
\beta_A = A \times Q \tag{4}
$$

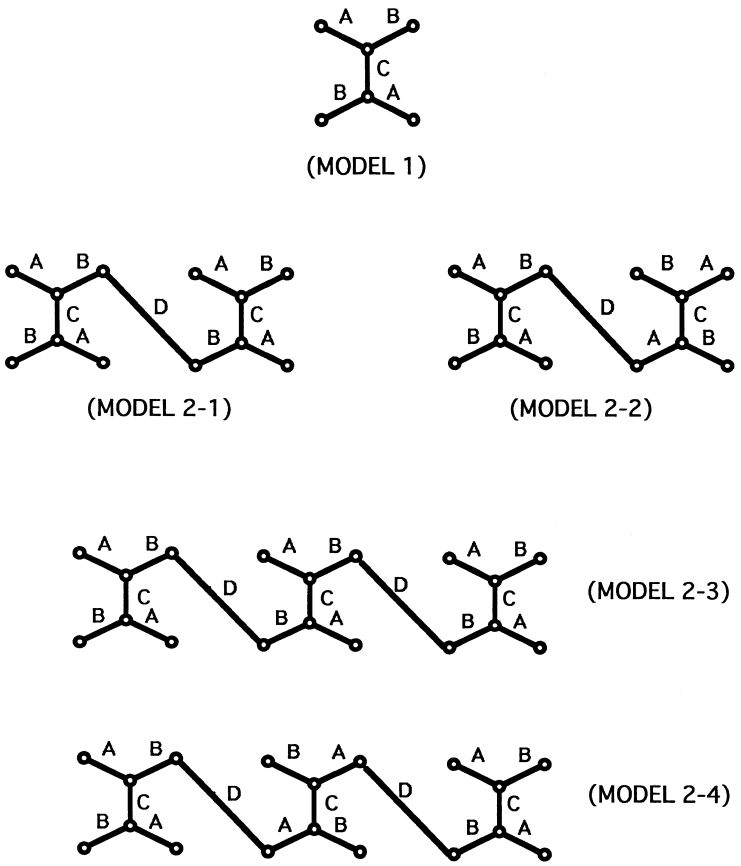

Fig. 5. Models for local structure of RNA in solution. A solid line in the models represents a partially double-stranded helix, a circle flexible region, and symbols A, B, C and D represent the length of a partially double-stranded helix.

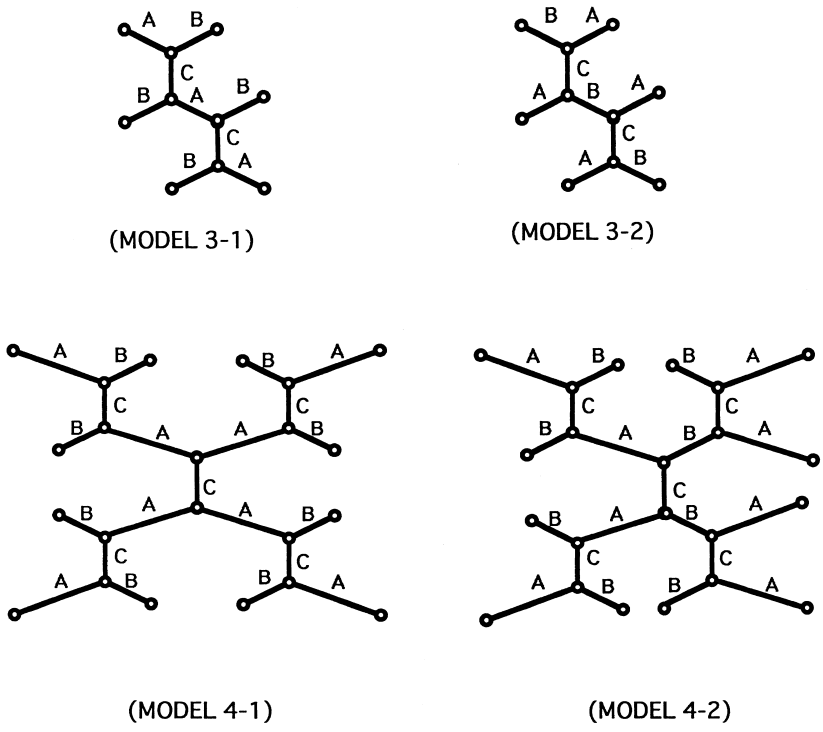

Fig. 5. (*Continued*).

$$\nu_C = \sin(\beta_C)/\beta_C \quad (5)$$

$$\Lambda(\beta_A) = \left(\frac{1}{\beta_A}\right)\int_0^{\beta_A}\frac{\sin t}{t}\,dt \quad (6)$$

etc.

Fig. 4-1 and 4-2 show such comparisons of the data DS-A and -B with theoretical curves for MODELs 2-1–2-4, respectively and Fig. 6-1 and 6-2 with those for MODELs 3-1–3-2 and 4-1–4-2, respectively. It is shown that the theoretical curves for MODELs 2-1–2-4 can satisfactorily mimic all observed plots, if the lengths A, B, C and D are

Table 2
Lengths of helical rods for structural models

C_p (mg ml^{-1})	S	Temp (°C)	MODEL 2-1,-2,-3,-4 (nm)				MODEL 3-1,-2, 4-1,-2 (nm)		
			A	B	C	D	A	B	C
4.5	0.2	20	10.5	10.5	5.5	36.0	12.0	12.0	8.0
4.5	0.2	30	10.5	10.5	7.0	38.0	12.0	12.0	11.0
4.5	0.2	40	11.0	11.0	7.0	39.0	12.5	12.0	11.0
4.5	0.2	50	11.5	11.5	8.0	40.0	12.5	12.5	12.5
4.5	0.2	20	10.5	10.5	5.5	36.0	12.0	12.0	8.0
3.32	0.05	20	10.5	10.5	5.5	36.0	12.0	12.0	8.0
3.12	0.025	20	10.5	10.5	5.5	36.0	12.0	12.0	8.0
2.95	0.003	20	10.5	10.5	5.5	36.5	12.0	12.0	7.0
5.764	Formamide	50	0	8	0	25			

assigned as given in Table 2, whereas those for MODELs 3-1 and 3-2 and 4-1 and 4-2 cannot afford to do so. Moreover, the upward turns of the scattering curves in the lowest-angle region, shown in Fig. 7 for DS-A, as an example, can be also reproduced by theoretical curves for MODELs 2-1–2-4, suggesting that these models could represent the structure of the RNA chain over a fairly large dimension.

The result for DS-A in Table 2 shows that, as the helical content decreases, the backbone structure of the RNA chain is still represented by MODELs 2-1–2-4 where the constituent rod lengths A–D are gradually increased. As the helix content decreases, unpaired bases should increase either at both ends of partially double-stranded helix (*Region*-A) or inside of the helix. In the former case, it is evident that increased unpaired bases would contribute to shorten the helical rod. In the latter case, however, the effect of increased unpaired bases on the structure would depend on how unpaired bases are distributed along the rod: if they are widely distributed and sufficiently far isolated from each other, they would contribute to lengthen the helical rod, because the mobility of the isolated unpaired bases would be so restricted by the adjacent paired bases and thus the original rigidity of the helical rod would not be significantly modified by an increase of the isolated unpaired bases and the pitch per one base along the axis of the helical rod would be longer in the unpaired state

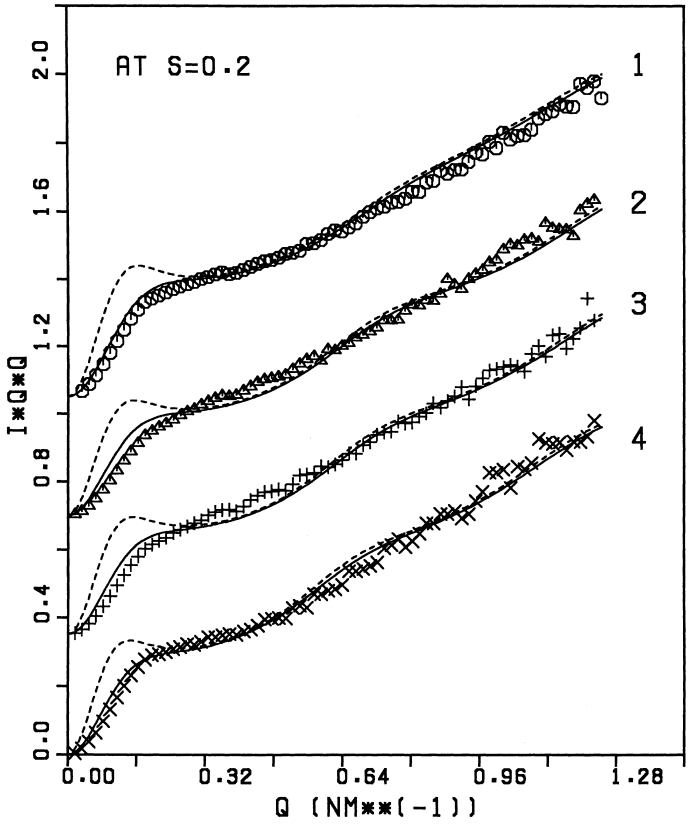

Fig. 6. (1) Comparison between the observed scattering curve of RNA in aqueous solution at 20°C (○), 30°C (△), 40°C (+) and 50 (×) and at fixed $S = 0.2$ and theoretical scattering curves for MODEL 3-1 (or 3-2) (solid curve) and MODEL 4-1 (or 4-2) (dotted curve). Rod lengths for the models are listed in Table 2. (2) Comparison between observed scattering curve of RNA in phosphate buffer solution at $S = 0.2$ (○), 0.05 (△), 0.025 (+) and 0.003 (×) and at fixed temperature of 20°C and theoretical scattering curves for MODEL 3-1 (or 3-2) (solid curve) and MODEL 4-1 (or 4-2) (dotted curve). Rod lengths for the models are listed in Table 2.

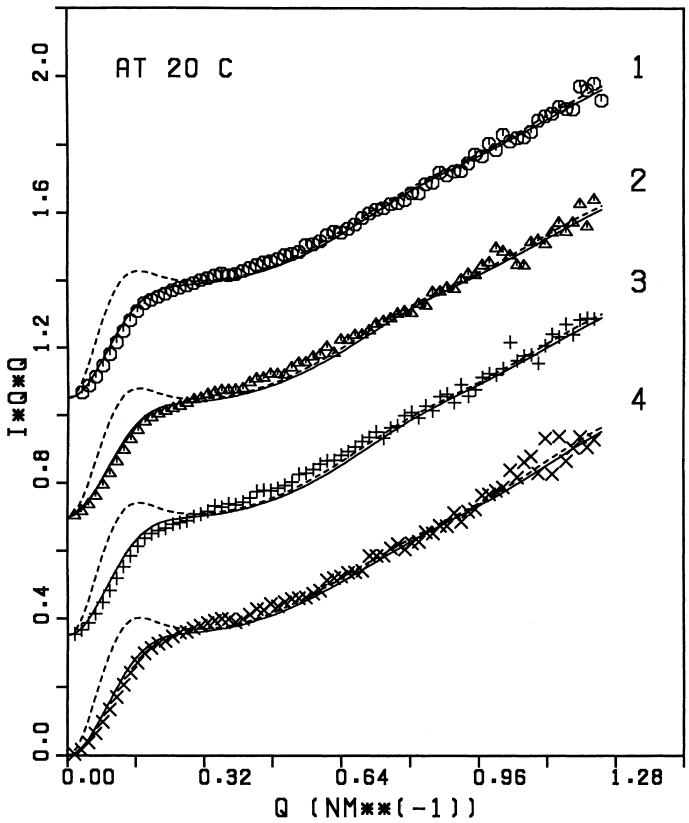

Fig. 6. (*Continued*).

than in the paired state. In this case therefore, the original feature of the structure should be preserved. On the other hand, if the increased unpaired bases are consecutively arranged along the helical rod and form another flexible region, the rod-like structure would be interrupted by the flexible region. In this case, the original feature in the structure should be gradually lost, as the helical content decreases. With these considerations, it is suggested that the local structure of the RNA chain in aqueous solution is characterized by an essential feature that unpaired bases in the partially double-stranded helix are constantly far isolated from each other along the helix and the rod-like structure of the helix is preserved over a range of helical contents.

On the other hand, in the case of DS-B, the backbone structure of the RNA chain is represented by MODELs 2-1–2-4 the constituent rod lengths of which are fixed over a wide range of S from 0.2 to 0.003 at 20°C, showing that the local structure of the RNA chain is quite stable against a change in S. Needless to say, the change in S should bring about perturbations in intermolecular interferences between different molecules, conformation of the chain in the flexible region (*Region*-B), structure of solvent, and ionic atmosphere around the RNA chain. However, the first perturbation would affect the scattering curve only in a lower scattering-angle region, and the second one would have a minor effect on the scattering curve, because each flexible chain in *Region*-B should have a comparatively short contour length, and the effects of the third one would be substantially eliminated by subtracting the scattered intensity of solvent from that of assem-

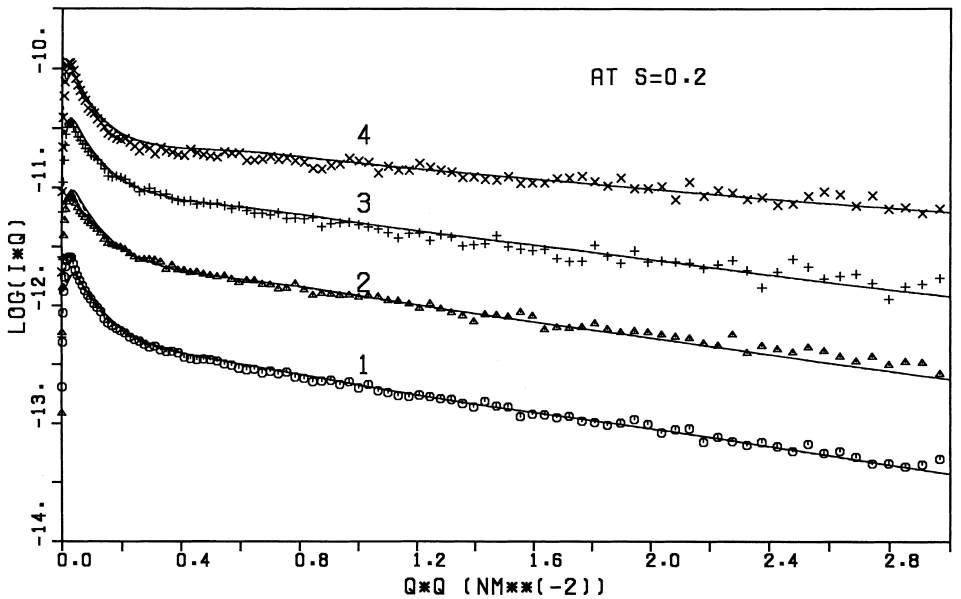

Fig. 7. Comparison between observed scattering curve of RNA in aqueous solution at 20°C (○), 30°C (△), 40°C (+) and 50°C (×) and at fixed $S = 0.2$ and theoretical scattering curves for MODEL 2-1 (or 2-2) (solid curve) and MODEL 2-3 (or 2-4) (dotted curve). Rod lengths for the models are listed in Table 2.

bly solution. A slight change in $\langle R_{cs}^2 \rangle^{1/2}$ listed in Table 1 may reflect an effect of the last perturbation on the local structure of the RNA chain.

As seen from Fig. 4-3 and Table 2, the backbone structure of the RNA chain in formamide at 50°C is represented by FHRs joined in series, not by FHRs joined in the form of a combination of the letter Y. This result clearly shows that the characteristic local structure of the RNA chain in aqueous solution is entirely collapsed in this media. However, taking into consideration that FHRs joined in series and a wormlike chain could give almost identical theoretical scattering curves if molecular parameters are suitably chosen, it still remains ambiguous which model, FHRs in series or a wormlike chain, is more proper to represent the local structure of the RNA chain in formamide at 50°C. Zipper et al. [29] have shown that the RNA chain from bacteriophage MS2 behaves as a wormlike chain in 4.6% formaldehyde at 60°C.

References

[1] P.J.G. Butler, J. Gen. Virol. 65 (1984) 253.
[2] R.N. Beachy, M. Zaitlin, Virology 81 (1977) 160.
[3] P. Goelet, J. Karn, Gene 29 (1984) 331.
[4] P. Goelet, G.P. lomonossoff, P.J.G. Butler, M.E. Akam, M.J. Gait, J. Karn, Proc. Natl. Acad. Sci. U.S.A. 79 (1982) 5818.
[5] T. Meshi, T. Ohno, Y. Okada, Nucleic Acids Res. 10 (1982) 6111.
[6] D. Zimmern, Nucleic Acids Res. 2 (1975) 1189.
[7] T.M.A. Wilson, K.A. Plaskitt, J.W. Watts, J.K. Osbourn, P.A.C. Watkins, NATO ASI Series H41 (1990) 123.
[8] R. Österberg, B. Sjöberg, R. Garrett, Eur. J. Biochem. 68 (1976) 481.
[9] J.W. Min, G. Haegeman, M. Ysebaert, W. Fiers, Nature 237 (1972) 82.
[10] H.F. Noller, C.R. Woese, Science 212 (1981) 403.
[11] R.W. Holley, J. Apgar, G.A. Everett et al., Science 147 (1965) 1462.
[12] R. Jacques, R. Fresco, B.M. Alberts, P. Doty, Nature 188 (1960) 98.
[13] Y. Muroga, Macromolecules 21 (1988) 2751.
[14] Y. Muroga, Macromolecules 25 (1992) 6063.
[15] Y. Muroga, Macromolecules 27 (1994) 2951.
[16] Y. Sano, Carbohydr. Polym. 33 (1997) 125.
[17] Y. Sano, Carbohydr. Polym. 38 (1999) 183.
[18] Y. Sano, J. Colloid Interface Sci. 139 (1990) 14.
[19] Y. Sano, Biopolymers 33 (1993) 69.
[20] Y. Sano, H. Inoue, Y. Hiragi, H. Urakawa, K. Kajiwara, Biophys. Chem. 55 (1995) 239.

[21] T.G. Northrop, R.L. Sinsheirmer, J. Chem. Phys. 22 (1954) 703.
[22] Y. Hiragi, H. Inoue, Y. Sano et al., J. Mol. Biol. 204 (1988) 129.
[23] Y. Hiragi, H. Inoue, Y. Sano, K. Kajiwara, T. Ueki, H. Nakatani, J. Mol. Biol. 213 (1990) 495.
[24] Y. Sano, H. Inoue, K. Kajiwara, H. Urakawa, Y. Hiragi, J. Biochem. 115 (1994) 1058.
[25] Y. Sano, H. Inoue, K. Kajiwara, Y. Hiragi, S. Isoda, J. Protein Chem. 16 (1997) 151.
[26] O.B. Ptitsyn, Visokomol. Soedin. 3 (1961) 1094, 1251.
[27] G. Porod, in: O. Glatter, O. Kratky (Eds.), Small Angle X-ray Scattering, Academic Press, New York, 1982, p. 32.
[28] P. Doty, H. Boedtker, J.R. Fresco, R. Haselkorn, M. Litt, Biochemistry 45 (1959) 482.
[29] P. Zipper, W. Folkhard, J. Appl. Cryst. 7 (1974) 168.